Nanoporous PBI Membranes by Track Etching for High Temperature PEMs

A. Eguizábal[1], M. Sgroi,[2] D. Pullini,[2] E. Ferain[3] M.P. Pina[1,4*]

[1]Instituto de Nanociencia de Aragón, Universidad de Zaragoza. Campus Rio Ebro, Edificio I+D, C/ Mariano Esquillor, s/n, 50018 Zaragoza, Spain

[2]Centro Ricerche Fiat, Strada Torino 50, 10043, Orbassano, Italy

[3]it4ip SA, rue J. Bordet (Z.I. C), 7180 Seneffe, Belgium

[4]Networking Research Center on Bioengineering, Biomaterials and Nanomedicine, CIBER-BBN, 50018 Zaragoza, Spain

Corresponding Author: tel. +34 976 761155, fax. +34 976 762776, e-mail: mapina@unizar.es

Abstract

This article describes for the first time the preparation of conducting track etched PBI membranes 25 mm thick with pore diameter values varying from 15 nm to 50 nm and overall porosity up to 10%. The TGA, DSC and FTIR characterization results for the so obtained nanoporous membranes reveal the chemical modification of PBI upon irradiation along the track walls. A clear conduction outperforming is shown by phosphoric acid doped track etched PBI in comparison with dense PBI counterparts. This behaviour could be explained by the effective contribution of additional pathways for proton transport involving shorter benzimidazole fragments, cross-linked PBI nanodomains and free amphoteric phosphoric acid molecules settled on the pore walls.

Keywords: track etching, polybenzimidazole, chemical modification, phosphoric acid doping, proton conductivity enhancement

1. Introduction

The development of economically feasible more efficient energy conversion systems is one of the most important technological challenges for the XXI century. The European Strategic Energy Technology (SET) Plan [1] has identified fuel cells and hydrogen among the technologies needed for Europe to achieve the 2020 targets. Much of the research on new materials for Polymer Electrolyte Membrane Fuel Cells (PEMFC), while promising, may be too far away from commercialization to meet this timeframe, and could be the next generation technology. Cost reduction seems to be the main challenge to a widespread PEM Fuel Cell commercialization, which is based on four main pillars with strong interdependencies: i) materials and manufacturing costs reduction through the use of new materials and novel fabrication approaches suitable for large scale production; ii) energy efficiency increase to reduce catalyst costs and equipment size through the use of new materials with improved properties or new concepts for stack configuration; iii) durability increase; and iv) fuel availability to become a real alternative to fossil fuels. Higher working temperatures would benefit PEMFC performance in terms of the balance of plant and the generation of more useful high-grade waste heat. Furthermore, fuelling options would become more flexible as the anode catalyst becomes more tolerant to impurities present in primary reforming streams. In addition, improvements in electro-kinetic performance will be expected at elevated temperatures where flooding of the electrodes is avoided. The term 'high temperature' refers to the temperature range, 100^{o}–200^{o}C (150^{o}-200^{o}C for some authors [3]) which does not appear to be high from an engineering point of view. However, in the current state of the art, development of high temperature PEM for fuel cells is very important in the field of materials science and engineering. Commercially available polybenzimidazole (PBI) has been the most extensively studied and used in membranes doped with all sorts of strong inorganic acids for high temperature PEMFC applications up to 200^{o}C [3-4]. This material has emerged as a well-known polymer due to is commercially available at a relative low cost (150-220 €/kg) and exhibits excellent thermal (Tg ≈ 425-435^{o}C; Td≈ 600^{o}C) and chemical stability in both reducing and oxidant environments. The conducting mechanism of phosphoric acid doped PBI membranes is based on the fact that the basic polymer acts as a proton acceptor, and an ion pair is formed, while phosphoric acid being amphoteric, is able to act both as proton donor (acidic) and proton acceptor (basic) to form dynamic hydrogen bond networks, in which protons are transferred by hydrogen bond breaking and forming processes [5]. Especially at temperatures below 100^{o}C, it is mainly controlled by Grotthus mechanism [3] involving proton transfer hopping between acid and water free molecules and protonated benzimidazole rings.

The main routes attempted to PBI upgrading by chemical modification could be resumed as follows: i) modification of the main chain by introduction of polar pyridine groups (improved chemical stability against oxidative degradation) [6], sulphone or ether groups (increased flexibility,

Con formato: Sin subrayado

Con formato: Sin subrayado

processability and solubility) [7-8], fluorine groups (excellent oxidative and thermal stability, high phosphoric acid uptake) [9], nitrile groups (improved ionic conductivity) [10]; ii) insertion of side chains as: N-phenyl 1,2,4-triazole (NPT) groups [11], bulky basic benzimidazole side groups [12], sulfophenyl sulfonyl groups [13], quaternary ammonium groups (QPBIs) [14]; iii) post-polymerization functional group insertion assisted by -NH groups of the imidazole rings (methyl and ethyl groups to increase solvent solubility, sulfonic groups to increase fire resistance) [15]; and iv) cross-linking to improve thermal and dimensional stabilities without decreasing proton conductivity [16].The approach herein attempted is not a conventional chemical modification of the PBI backbone but a post-casting porosification procedure also responsible for chemical modification of the main PBI chain along the track walls. In particular, ordered nanoporous PBI films characterized by straight passing pores perpendicular to the membrane itself have been prepared by track-etching. The heavy ion irradiation (energy of the order of several MeV) of PBI followed by the chemical etching is the object of this investigation. It has been approximately five decades [17-18] since researchers first began exposing materials like polymers to ionizing radiation, and reporting the occurrence of cross-linking and other useful effects. This technique offers the possibility to obtain very high aspect ratio (up to 1000) structures and better conditions for producing high-density (even $>10^9$tracks per cm^2) at the expense of high irradiation cost [19-20]. So far, the track formation and etching process has been studied in much detail for several polymeric materials. In general, pore dimensions are controllable and depend upon various factors: the nature and energy of incident particles, the target material, chemical etching conditions (temperature, nature of etchant, pre-etch storage conditions) [21-26]. Today, track-etching technology maturity enables the manufacturing of any particular product based on polyethylene terephthalate (PET), polycarbonate (PC)and polyimide (PI).Applications of commercially available track-etched membranes are mainly in the fields of micro-organism retention, cell detection and culture, and laboratory filtration [19].However, by proper chemical modification of the nanopores, retention and transport properties of track-etched membranes are no longer fixed by the choice of substrate material [27-28].

This article describes for the first time the preparation of conducting PBI track etch, denoted as TE for the remainder of the work, membranes for PEM applications with the final purpose of proton transport promotion over dense PBI counterparts. Unlike our previous works where randomly porous PBI membranes have been prepared either by leaching out a low-molecular-weight compound [29] or inverse phase method [30]; the passing through nanopores herein obtained, are expected to improve the conductivity of phosphoric acid doped nanoporous PBI. Nevertheless, special attention has to be devoted to fuel cross over phenomena, especially if anodic and cathodic pressures are not well balanced. For such reasons, thin layer of dense PBI could be deployed as diffusional barriers to reduce fuel cross-over and, at the same time to alleviate the conductor leakage/dragging with time

Con formato: Sin subrayado

on stream. The low thickness for the dense polymer film should render in low ohmnic polarization drop; thus, prevailing the benefits of the straight pore conducting membrane. Kros et al. [31] described the confined polymerization of organic conducting monomers (thiophenes, pyrrole) inside the nanopores of TE membranes for the development of biosensors. They reported improved electrical properties compared to their corresponding bulk materials due to the alignment of the conducting polymers along the transport axis. Unlike Kros´ approach, in this work TE polybenzimidazole membranes are impregnated with phosphoric acid as conducting material for two main purposes: i) doping of the basic polymer backbone; and, ii) nanoreservoirs filling with free phosphoric acid. The final result is the acid-base H_3PO_4-PBI ordered support with its nanopores containing highly conducting molecules. Thus, superior proton conduction performance is expected due to additional and shorter pathways for proton transport are provided through free phosphoric acid molecules confined in the ordered channels connecting both membrane sides. Firstly, the track-etching process parameters, mainly irradiation time and chemical etching conditions, have been optimized to identify the best combination for thin film PBI membranes. Once the operation-window conditions are defined, the second part of this work has been devoted to the characterization of the successfully prepared nanoporous PBI by step along the track-etching process to assess about any physico-chemical modification. Finally, the proton conduction performance of TE PBI membranes after phosphoric acid doping has been evaluated up to 200^{o}C and compared with those exhibited by dense PBI counterparts.

2. Experimental

2.1 Dense PBI Casting

Poly[2,2-(m-phenylene)-5,5-bibenzimidazole] (PBI) dense films were prepared from commercial Fumion APH (190 kDa) powder according to the procedure described elsewhere [18]. Mainly, 0.5 g of PBI powder, 0.01 g of LiCl, as stabilizer, and 9.3 g of N-N dimethylacetamide (DMAc) are mixed in the autoclave under autogenous pressure at 240 ^{o}C for 24 h to obtain a PBI solution of 5 % wt in DMAc. Before use, the PBI solution is filtered to remove insoluble solids from the starting PBI powder. The mixture is poured onto a glass plate of 14 cm in diameter preheated to 60 °C, in an electrical oven without convection. A heating rate of 10 °C/h is kept up to 90 °C and the membrane is maintained at this temperature for 12 hours to ensure the solvent evaporation. The dried membranes are peeled off by addition of DDW. Then, LiCl stabilizer is removed by successive membrane immersion cycles into boiling DDW during 2 h. A series of dense films with controlled thickness between 25 and 50 μm has been obtained. The residual solvent (DMAc) is finally removed by evacuation (2 mbar) at 80^{o}C during 24 hours. A series of free-standing, homogeneous, translucent brown membranes with controlled thickness (25-50 μm) has been obtained.

Con formato: Sin subrayado

2.2 *Track-etching Process*

Track-etching is a two-step process consisting in: i) an irradiation of a thin polymeric film by energetic heavy ions creating linear damage tracks; ii) followed by a selective chemical etching of these tracks into pores (see Fig 1).All the nanoporous PBI membranes herein prepared were irradiated under vacuum with 420 MeV Xe ions (Cyclotron Research Centre at Louvain-la-Neuve, Belgium). At this energy, Xe ions can efficiently cross a 40 µm thick dense PBI film; beam intensity and beaming time were therefore chosen to reach a final pore density from 1,00E+09 to 5,00E+09 cm^{-2}.

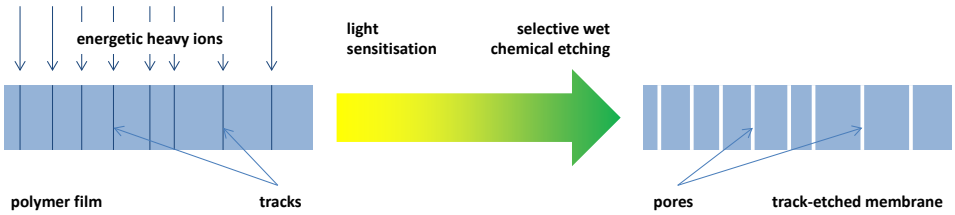

Figure 1. Track-etching process for the production of porous membranes from polymer films.

An optional light sensitisation step can be performed prior to etching to further modify the polymer along ion tracks. It has been shown that high polarity compounds are thereby created along tracks into a polycarbonate film, improving etchant diffusion and therefore track-etching selectivity [21-22]. Combined to etching conditions, sensitisation parameters can be monitored to reach a controlled pore shape. For PBI films, an efficient track sensitisation has been performed in blue visible range and pore development has been considered by immersion into different alkaline solutions (KOH, NaClO). DMAc was also tested on the basis of their excellent solvent properties. Thus, PBI was etched for 1 hour in a three-neck round bottom flask immersed in a thermostatic bath at 70º, 80º,90º or 100ºC under reflux and inert atmosphere. Afterwards, PBI samples were thoroughly washed by successive membrane immersion cycles into boiling DDW and evacuated (15 mbar) at 80ºC for at least 24h before storage.

2.3 *Phosphoric Acid Doping*

Finally, the TE PBI samples were subjected to H_3PO_4 acid doping for proton conduction purposes. In particular, nanoporous PBI films were immersed in 11 M acid solutions for more than 24 hours at 80ºC under mechanical stirring, dried with blotting paper and finally evacuated (15 mbar) at 80ºC for at least 4 h. The phosphoric acid doping levels (mole number of H_3PO_4 per repeat unit of

Con formato: Sin subrayado
Con formato: Sin subrayado
Con formato: Sin subrayado
Con formato: Sin subrayado
Con formato: Sin subrayado

PBI) here reported have been calculated for membranes 4 cm^2 in surface from the weight differences between doped membrane "m_{doped}" and without doping "m_p". Thus, the herein reported phosphoric acid doping levels have been somewhat overestimated due to the hydrophilic properties of the membranes (i.e. water uptake values above 16% wt.). In addition, thermogravimetric analyses (TGA) from room temperature up to 900 ºC under N_2 flow and using 1 ºC·min^{-1} as heating rate, were performed over 0.25 cm^2 samples with a Q5000 IR TGA (TA Instruments) for phosphoric acid and water quantification purposes.

Con formato: Sin subrayado
Con formato: Sin subrayado
Con formato: Sin subrayado
Con formato: Sin subrayado
Con formato: Sin subrayado
Con formato: Sin subrayado

2.4 Characterization Techniques

ATR-FTIR analyses (VERTEX 70 equipment with microscope slide MKII Golden Gate ATR from 4000 to 600 cm^{-1}, 256 scans and resolution of 0.05 cm^{-1}) were performed onto PBI membranes throughout the track etching process, that means: i) after casting, ii) after ion beaming, and iii) after chemical etching; to study any chemical surface modification. Spectra were collected by cumulating 256 scans at a resolution of 5 cm^{-1}. Similarly, differential scanning calorimetry (DSC, Mettler Toledo DSC822^e) analyses from room temperature up to 600 ºC at 5 ºC·min^{-1} as heating rate, were also carried out for thermal properties assessment with porosification process.

Morphology, thickness and homogeneity of the as prepared membranes have been studied by electron microscopy techniques. The end diameters (i.e., as measured at the top surface) were measured by SEM (InspectTM F50) and environmental SEM (Quanta FEG 250). In addition, better resolution TEM (TECNAI T20) images of electron transparent PBI slices obtained at different distances to the top surface have also been performed to assess on pore diameter through the PBI thickness.

The existence of passing pores connecting both sides of PBI membranes was assured by permeation measurements. Attempts to estimate pore volume and pore size distribution by N_2 physisorption measurements (ASAP 2020) were failed due to the low porosity of the as prepared samples (below 0.006 cm^3/g for PBI_30_0.7) and the proximity of the relative pressure values required for N_2 physisorption in such mesopores (circa 0.935 for PBI_30_0.7) to capillary condensation phenomena.

Proton conductivity measurements of nanoporous doped PBI membranes were performed in a homemade cell [32] under 100 cm^3 N_2 STP/min up to 200ºC using 0.5ºC·min^{-1} as heating rate. Considering water is the unavoidable by-product of PEM fuel cell reaction, all the conductivity tests were carried out in presence of 0.05 water molar fraction. Conductivity values were calculated from electrochemical impedance spectra using an Agilent 4294A Precision Impedance Analyzer.

3. Results and discussion

3.1 Optimization of track etching conditions for PBI based membranes

Table 1 summarizes the etching conditions studied for 50 μm thick PBI films after ion beaming at $1 \cdot 10^9$ ions/cm^2. As it can be observed, KOH based etching (1M, 2M, water and ethanol as solvents, 70ºC to 100ºC) does not succeed in pore formation. On the other hand, samples were destroyed by DMAc at temperatures above 80°C due to the simultaneous bulk and damaged material etching. Sodium hypochlorite has been deeply studied to gain control over the etching process (i.e., rate and aspect ratio) on PI films [23-26]. Aqueous solutions of NaClO rapidly decomposes as a function of pH, light, temperature. According to Klintberg [25] the final shape and size of the pores are determined by the combination of NaClO content and pH. In this work, successfully etching of latent tracks in PBI was achieved using NaClO aqueous solution (from 0.3 M to 2.0 M) at pH 9.5 and at 65° for more than 40 min depending of the required final pore size. According to this chemical etching procedure, the main characteristics of the nanoporous PBI membranes herein prepared are shown in Table 2. The nomenclature describes the pore size and the porosity, thus PBI_30_0.7 corresponds to samples 30 nm in pore size and 0.7% in porosity. As it can be observed, different porosities ranging from 0.7% to 10% are obtained by modifying either the beaming conditions (i.e. pore density from $1 \cdot 10^9$ to $5 \cdot 10^9$ cm^{-2}) or the chemical etching conditions (i.e. pore diameter from 15 nm to 50 nm). Nevertheless, the random pore distribution in plane is the key factor determining is the maximum affordable porosity of the PBI material. In an attempt to increase pore diameter and pore density, harsher beaming and etching conditions were assayed. Unfortunately, at high pore density, the probability of pores coalescence increases and also the fragility of the membranes. Accordingly, the maximum porosity successfully achieved in this work is 10%.

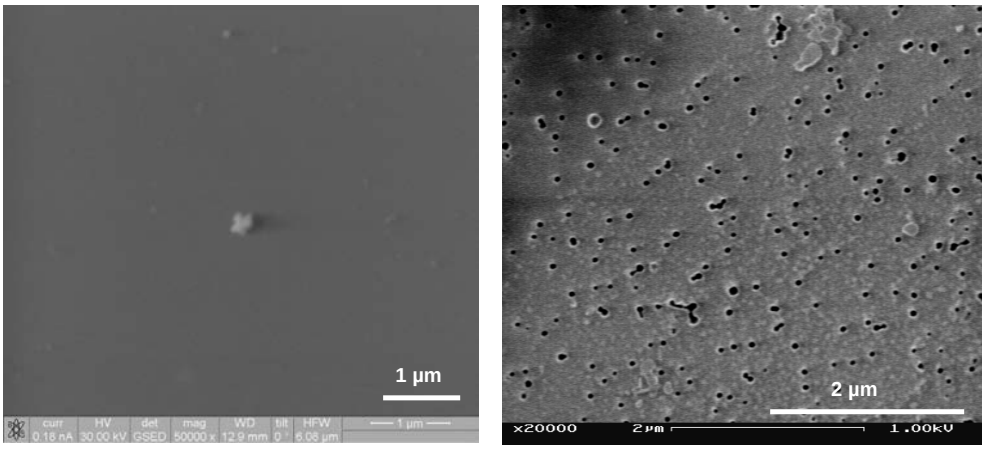

Figure 2. PBI films 50 μm thick after chemical etching: left) 2M KOH solution at 80ºC; right) 2M NaOCl solution at 65ºC.

Con formato: Sin subrayado

Table 1. Screening of Chemical Etching Conditions for 50 μm thick PBI films beamed at $1 \cdot 10^9$ ions/cm^2.

Etching Conditions	1 M KOH (60 min)	2 M KOH (60 min)	2M KOH + 10% Ethanol (60 min)	DMAc (60 min)	NaClO 2.0 M at pH 9.5 (200 min)
70°C	No pores	No pores	No pores	No pores	No pores
80°C	No pores	No pores	No pores	Dissolution	--
90°C	No pores	No pores	No pores	--	--
100°C	No pores	No pores	No pores	--	--

Table 2. Track-etched PBI membranes successfully prepared in this work.

Samples	Ion Beaming Conditions	PoreDensity (cm^{-2})	Etching Conditions	Mean Pore size (nm)*	Nominal Porosity (%)
PBI_30_0.7	Xe 420 MeV	$1 \cdot 10^9$	NaClO1.0M/pH 9.5/65°C/60min	30	0.7
PBI_15_0.7		$4 \cdot 10^9$	NaClO 0.3M/pH 9.5/65°C/80min	15	0.7
PBI_30_3.5		$5 \cdot 10^9$	NaClO 0.6M/pH 9.5/65°C/90min	30	3.5
PBI_50_10		$5 \cdot 10^9$	NaClO 2.0M/pH 9.5/65°C/45min	50	10

*estimated by permeation measurements considering Knudsen diffusion regime

3.2 Morphological and Physico-chemical characterization characterization of track-etched PBI membranes

Environmental SEM micrographs for TE membranes as a function of pore density and pore size are shown in Figure 3. TEM images for PBI_30_0.7 and PBI_15_0.7 samples are shown in Figure 4 to illustrate the pore size variation with the distance to the top surface. According to such observations, the estimated end diameters are 35 nm and 15 nm for PBI_30_0.7 and PBI_15_0.7 respectively. Ideally, a feature of track-etch preparation technique is that the pores are uniform cylinders traversing the membrane at right angles. However, the pore diameters in TE PBI films are changing in size and shape with depth due to tracks coalescence. In fact, some pores with 278 nm x 166 nm and 57nm x 38 nm are encountered at 10 μm to the top surface for PBI_30_0.7 and PBI_15_0.7samples respectively. Accordingly, the PBI membrane porosity should be kept lower than 0.7% to minimize the formation of multiple holes produced when many nucleation tracks are closed together. The mechanical properties of irradiated samples are commonly evaluated by the load-deflection method. For TE membranes prepared following similar procedures, the burst pressure for 1 cm^2 of unsupported sample is usually above 2.5 bar. In our case, the mechanical properties were not tested after phosphoric acid doping; but no major differences will be expected on the basis of their low porosity values.

Con formato: Sin subrayado

Con formato: Sin subrayado

Con formato: Sin subrayado

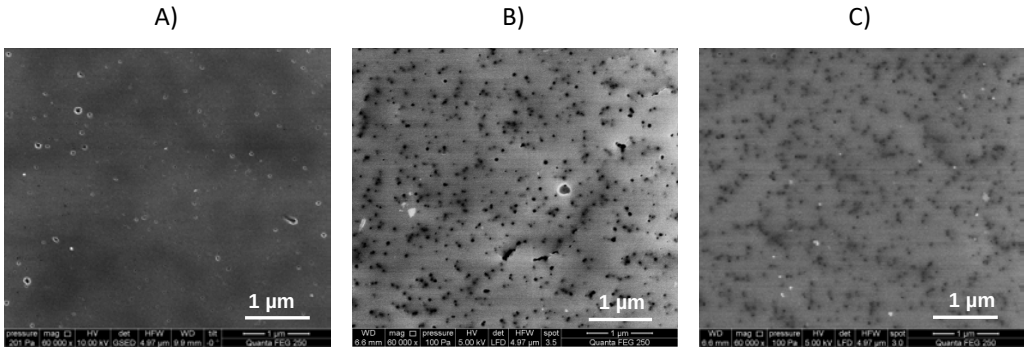

Figure 3. Top view of nanoporous TE PBI membranes: A) PBI_30_0.7; B) PBI_30_3.5; B) PBI_50_10

Con formato: Sin subrayado

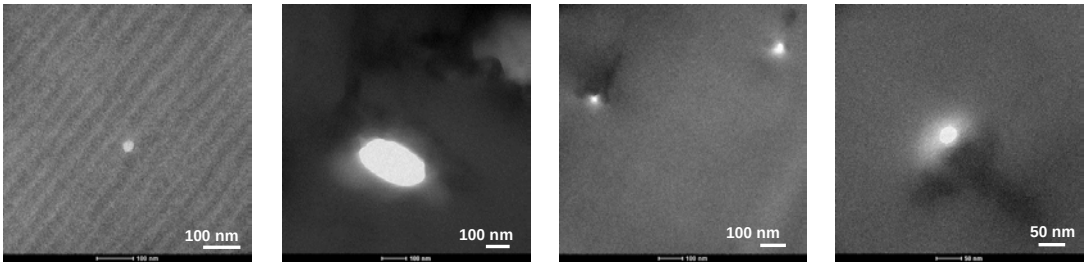

Con formato: Sin subrayado

Figure 4. TEM analyses of pore size variation with the depth in the PBI_30_0.7 sample: A) top surface, B) 10 µm to the top surface; and the PBI_15_0.7 sample: C) top surface, D) 10 µm to the top surface.

FTIR spectra of TE PBI samples are depicted in Figure 5.A (1550-1150 cm^{-1} region), Figure 5.B (1050-750 cm^{-1} region) and Figure 5.C (3700-2900 cm^{-1} region). The characteristics FTIR assignments for PBI are clearly observed. However, the relative intensities for the main bands are modified by track etching processing. We tend to attribute these differences to physico-chemical variations of the polymer backbone along the trajectories of highly energetic Xe ions. In general, ion irradiation is thought to modify the polymeric networks [33] according to three different processes, whose contribution depends on the transferred energy density and on the type of the irradiated polymer. The mechanisms are the following: i) shock wave induced plastic deformation of the ion track environment; ii) chain-scission; and, iii) radiochemical bonding of neighbouring polymer chains i.e., cross-linked chains forming aggregates in the surroundings of ion tracks. Some authors have described the coexistence of alternating high density nanosized regions and low density ones onto PI

samples as a consequence of heavy ion tracking exposure [34]. In our case, we attribute the dark brownish appearance of TE PBI membranes, compared to pristine PBI, to such cross-linking effect and not to the presence of nanometric pores.

As it is well known from the TE polyimide related literature [23-24, 26], the irradiation of PI films results in the scission of imide cycles with the formation of amide groups and intermolecular crosslinks. In the case of PBI, the FTIR spectra evolution (see Figure 5.A) agrees with the PBI chain scission rendering in benzimidazole fragments. In fact, the intensity values for the characteristic peaks at 1222 cm^{-1} and 1528 cm^{-1}, corresponding to the in-plane C-H deformation of 2,6-disubstituted benzimidazole and in-plane ring vibration of 2 disubstituted benzimidazole, respectively; increase for irradiated samples. These observations are even more remarkable as the pore density increases from $1 \cdot 10^{9} cm^{-2}$ (sample PBI_30_0.7), up to $5 \cdot 10^{9}$ cm^{-2} (samples PBI_30_3.5 and PBI_50_10). In addition, the characteristic band at 1443 cm^{-1}, corresponding to the in-plane ring vibration of 2,6-disubstituted benzimidazoles, widens and shifts towards higher wavenumber values. Thus, the higher vibration energy value is due to the presence of polymeric clusters with low free volume where short-chain mobility is inhibited. However, these high density nanosized regions alternate with low density ones (i.e. higher free volume) where randomly arranged chains are prevailing. In fact, these disordered nanodomains of shorter chains are responsible for the FTIR peak intensity enhancement at 3402 cm^{-1} belonging to “free” non hydrogen bonded N-H stretching (see Figure 5.C).

The intensity values for the characteristic peaks at 802 cm^{-1}, 902 cm^{-1} and 1017 cm^{-1}, corresponding to the heterocyclic ring vibration or C–H out-of-plane bending of three adjacent hydrogen atoms in substituted benzene rings, C–H out-of-plane bending of a single hydrogen in substituted benzene rings, and benzene-ring vibration; are clearly diminished and shifted towards high energy values with pore density (see Figure 5.B). The observed behaviour agrees with the PBI scission through the benzimidole-benzene rings and the appearance of –C-H bonds. Indeed, this explanation correlates with FTIR band intensity enhancement at 3050 cm^{-1} belonging to aromatic C-H stretching (see Figure 5.C).

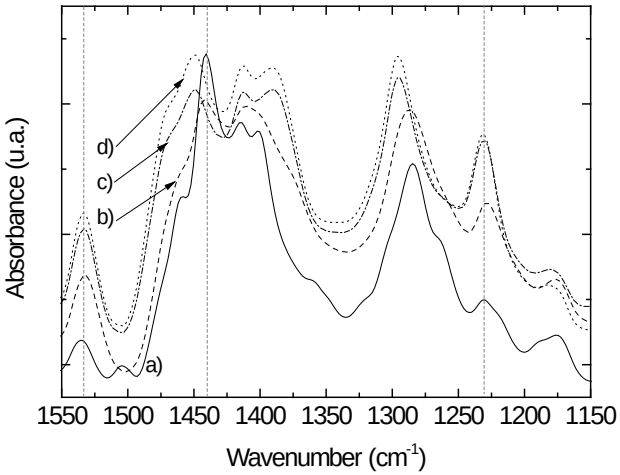

Figure 5.A. FTIR analysis in the 1550-1150 cm^{-1} region for TE PBI membranes with different pore density values: a) pristine PBI; b) PBI_30_0.7 ($1 \cdot 10^9$ cm^{-2}); c) PBI_30_3.5 ($5 \cdot 10^9$ cm^{-2}); d) PBI_50_10 ($5 \cdot 10^9$ cm^{-2}).

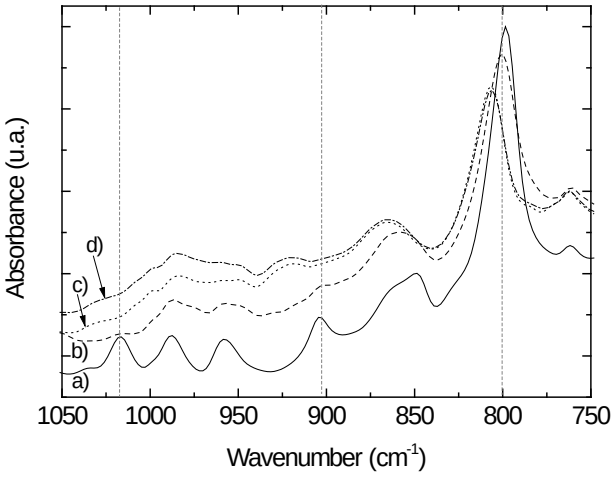

Figure 5.B. FTIR analysis in the 1050-750 cm^{-1} region for TE PBI membranes with different pore density values: a) pristine PBI; b) PBI_30_0.7 ($1 \cdot 10^9$ cm^{-2}); c) PBI_30_3.5 ($5 \cdot 10^9$ cm^{-2}); d) PBI_50_10 ($5 \cdot 10^9$ cm^{-2}).

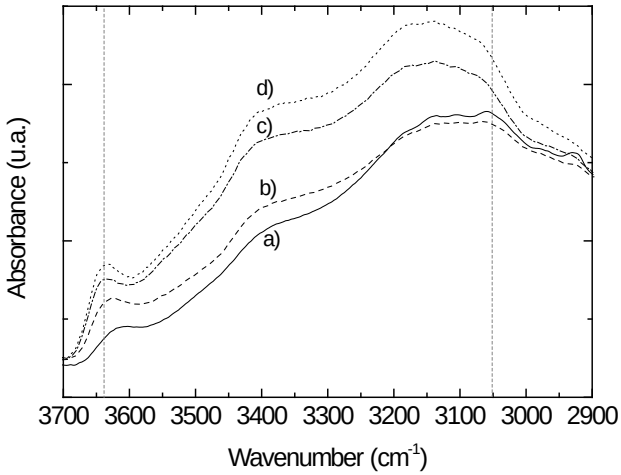

Figure 5.C. FTIR analysis in the 3700-2900 cm^{-1} region for TE PBI membranes with different pore density values: a) pristine PBI; b) PBI_30_0.7 ($1 \cdot 10^9$ cm^{-2}); c) PBI_30_3.5 ($5 \cdot 10^9$ cm^{-2}); d) PBI_50_10 ($5 \cdot 10^9$ cm^{-2}).

DSC studies on irradiated PBI samples reveal the modification of the plastic behaviour of the polymer with the track-etching process as shown in Figure 6.A. The first endothermic event, below 150ºC and reported for all the samples, corresponds to water desorption. More noticeable is the glass transition temperature (Tg) shift to lower values for TE membranes. In particular, the evaluated Tg values (using 20 ºC/min as heating rate for DSC analysis) are 272 ºC and 402 ºC for PBI_50_10 and pristine PBI, respectively. This observation is explained by the chain scission phenomena leading to shorter polymer chains with better mobility.

DSC analysis of PBI_50_10 sample (using 5ºC/min as heating rate) after beaming and after chemical etching are comparatively shown in Figure 6.B to underline the presence of carbonaceous deposits by-products. As it was expected, the decomposition events are clearly anticipated for samples only exposed to heavy ion irradiation (T_d=560ºC for TE sample vs. T_d=600ºC for dense PBI). This phenomenon corresponds to the degradation of the small polymeric fragments that loosely remain on the irradiated film. However, such carbonaceous material is completely removed from TE membranes during the hypochlorite etching. Afterwards, the nanoporous supports recover the decomposition behaviour recorded for pristine PBI.

Con formato: Sin subrayado

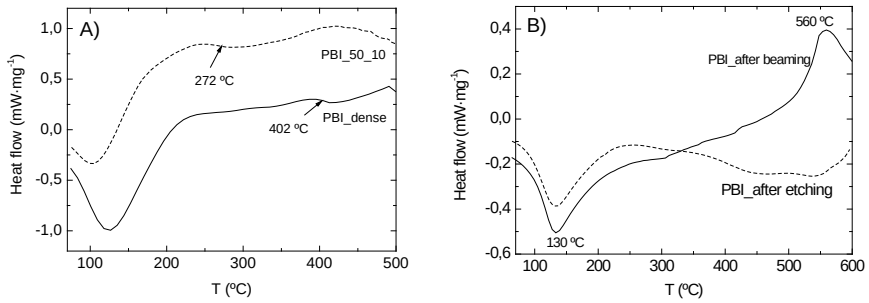

Figure 6. DSC analyses for some of the TE PBI membranes prepared in this work: A) Influence of track etching on Tg values; B) Removal of carbonaceous by-products generated during beaming with chemical etching step.

Con formato: Sin subrayado

3.3 Phosphoric Acid Doped TE PBI membranes: characterization and postulated proton conduction mechanism

Table 3 summarizes the TE PBI films composition evaluated by TGA after immersion for 24 h in 11 M phosphoric acid solutions at 80ºC and finally evacuated (15 mbar) at 80ºC for at least 4 h. Pristine PBI is also included for comparison purposes. SEM images of the top surface for PBI_30_0.7 as a function of doping time are shown in Figure 7. A phosphoric acid gel-type layer on the membrane top surface is clearly distinguished from the micrographs. In fact, the presence of such skin phosphoric layer makes difficult the SEM monitoring of the nanopores filling with doping time.

Only when ion beaming becomes remarkable, i.e., pore density of $5 \cdot 10^9$ cm^{-2}, the H_3PO_4/PBI ratio clearly exceeds the one of the pristine case, above two folds higher than reference. For a given end pore diameter of 30 nm, the phosphoric acid content increases from 40.4% to 56.9% wt. when nominal porosity varies from 0.7% ($1 \cdot 10^9 cm^{-2}$ as pore density) to 3.5% ($5 \cdot 10^9 cm^{-2}$ as pore density). TEM observations (see Figure 4) reveal the tracks coalescence as the pore density increases. However, phosphoric uptake values are still clearly superior to those required for the filling of the nanopores. We tend to hypothesize that such values are not only due to the presence of pores as acid containers. The physico-chemical variations of PBI in the surroundings of the latent tracks are playing a key role on the phosphoric acid embedding process. Based on FTIR analyses, our explanation relies on the fact that the chain scission provoked by ion beaming becomes more noticeable with pore density. Thus, the generation of low density regions with randomly arranged benzimidazole fragments in the vicinity of the tracks not only facilitates, but also enhances the phosphoric acid uptake by free –NH groups with distinct basic character.

A) B)

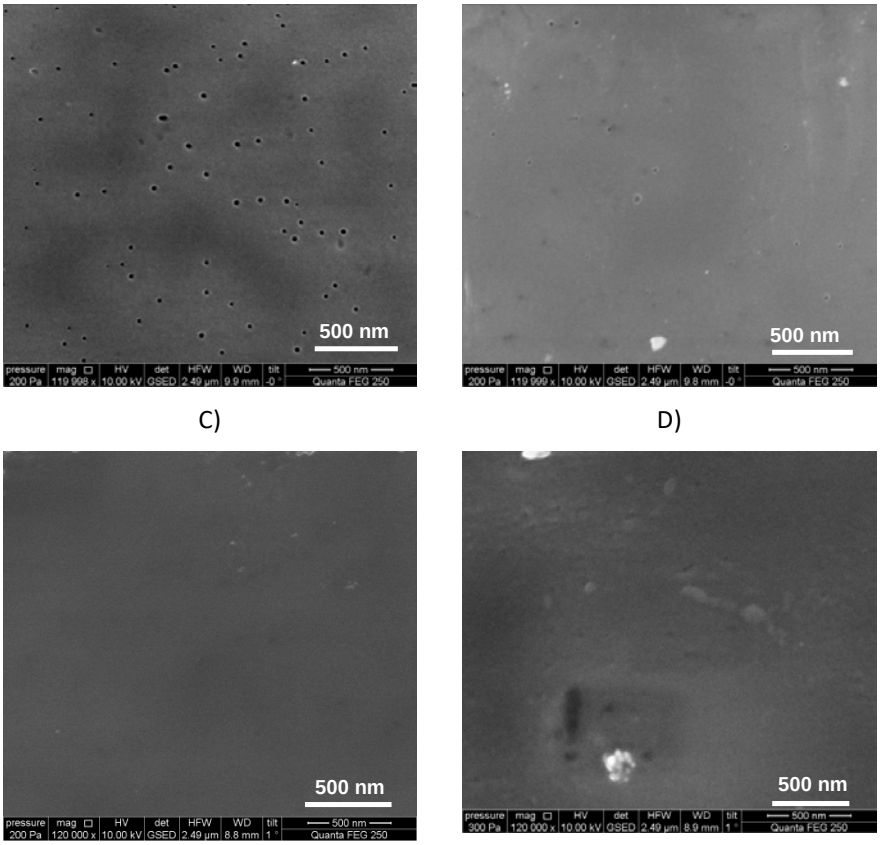

Figure 7. Top view of phosphoric acid doped PBI_30_0.7 membrane as a function of doping time: A) 0 h; B) 0,5 h; C) 6h; D) 24 h (pore coalescence is observed).

Con formato: Sin subrayado

Table 3. Doping levels and H_3PO_4 uptake values for the TE PBI membranes prepared in this work.

Sample	TGA estimations		Doping level (mol(H_3PO_4)/mol(PBI))***
	H_3PO_4 (wt.%)*	H3PO4/PBI (wt. ratio)**	
PBI_dense	42.3	1.2	10.4
PBI_30_0.7	40.4	1.0	16.8
PBI_15_0.7	41.7	1.1	16.6
PBI_30_3.5	56.9	2.2	17.3
PBI_50_10	58.6	2.7	18.1

$$*H_3PO_4\,(\%) = 100 \cdot \frac{m_{H_3PO_4}}{m_{PBI}+m_{H_3PO_4}+m_{H_2O}}$$

$$**\frac{H_3PO_4}{PBI} = \frac{m_{H_3PO_4}}{m_{PBI}}$$

$$***Doping\ level = \frac{m_{doped}-m_0}{m_0} \cdot \frac{MW(PBI)}{MW(H_3PO_4)}$$

This hypothesis is also supported by the differential TGA shown in Figure 8 for doped PBI and PBI_50_10 ($5{\cdot}10^9 cm^{-2}$ as pore density) samples respectively. In agreement with DSC analyses, the plastic deformation induced by ion beaming shifts the PBI decomposition/degradation peak from 820°C to 702°C. In the case of water molecules, the desorption of weakly bonded molecules takes place at temperatures below 100°C, whereas strongly bonded molecules are released at temperatures around 150°-170°, overlapping with the oligomerization of phosphoric acid. For this intrinsic conductor, two main peaks at 160 °C and 600°C corresponding to the 1st and 2nd dehydration of phosphoric acid molecules are clearly distinguished in the reference PBI. On highly irradiated samples, two new shoulders appear at 263° and 339°C respectively. However, the most noticeable effect is the 2nd phosphoric acid dehydration band enlargement and shift to lower temperatures (i.e. 541°C). Both observations could be explained by: i) the existence of additional proton donor sites with dissimilar nature; and, ii) the extra contribution of "free" acid molecules along the pore walls.

Con formato: Sin subrayado
Con formato: Sin subrayado
Con formato: Sin subrayado
Con formato: Sin subrayado
Con formato: Sin subrayado
Con formato: Sin subrayado

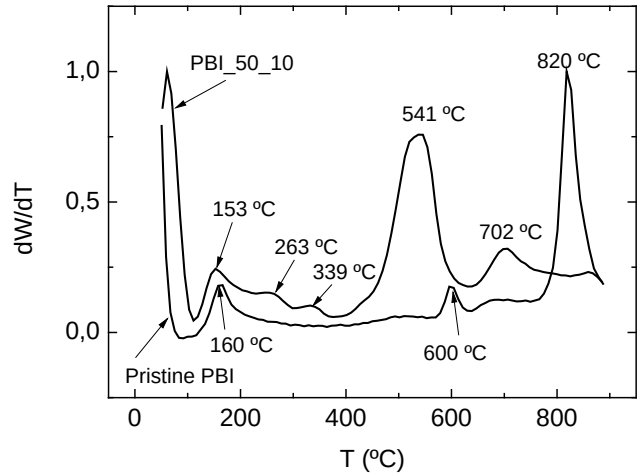

Figure 8. Differential TGA for phosphoric acid doped PBI_50_10 and pristine PBI samples.

Unlike highly nanoporous membranes, TE samples 0.7% in porosity exhibit phosphoric acid loadings similar to unirradiated PBI, around 40% wt. This observation could be explained by a dominant contribution of the bulk polymer doping. On the contrary, the doping levels for the same membranes estimated by weighting are above 6 points over pristine PBI. We attribute these apparent discrepancies to the sample heterogeneity. Mainly, the difference in the sample amount used for both type of estimations (below 4 cm^2 for gravimetry and around 0.25 cm^2 for TGA) makes difficult the comparison. The higher quantity used for the doping level estimation dilutes the sample heterogeneity effect (irregular tracks distribution and random pore size variations along the thickness) on such macroscopic property.

Accounting from that, the doping level data evaluated by weighting are considered more meaningful for the remainder of this work. Nevertheless, it is worthwhile to mention that such acid doping levels are clearly overestimated (see Section 2.3). By this technique, the phosphoric acid doping level increases on average in a 64% and 74% (referred to unirradiated PBI) for TE samples with 0.7% and 10% in porosity, respectively. As previously described, those values are not only due to the presence of pores as acid containers but also to the physico-chemical variations of PBI in the surroundings of the latent tracks. Particularly, the PBI chain scission and cross-linking, with opposite effects on phosphoric acid uptake values have to be considered for a proper explanation of the encountered results. The radiochemical PBI cross-linking in the surroundings of tracks is negatively affecting its phosphoric acid doping due to the reduction in the intermolecular spaces between chains.

Con formato: Sin Resaltar

Con formato: Sin subrayado

Con formato: Sin subrayado

On the contrary, the chain-scission renders in a higher amount of phosphoric acid anchoring sites with dissimilar basic character.

The conduction performance for the as prepared TE PBI membranes is shown in Figure 9 at 50º, 100º, 150º and 200ºC as a function of doping levels. Unirradiated PBI sample has also been included as baseline. As it was expected, the through-plane proton conductivity always increases with doping level. Consequently, the conductivity properties of irradiated samples clearly outperform the exhibited by pristine PBI. Conductivity values above 22 mS/cm are reported for PBI_50_10 at 150ºC in comparison with 12 mS/cm for pristine PBI. However, the conductivity values herein obtained are lower than those reported in literature for similar doping levels (i.e 80 mS/cm at 150ºC for PBI membrane cast from 105.1 kDa polymer and 14.5 as doping level [35]). These differences are attributed to the overestimated acid doping levels due to water sorption. On the basis of H_3PO_4/PBI molar ratio calculated from H_3PO_4/PBI wt ratio estimated by TGA analyses (see Table 3), the exhibited conductivities agree quite well with SoA data. As an example, the so obtained doping level for PBI_dense sample would be 3.8, around 36% of the value shown in Table 3 and Figure 9. In fact, this doping level correlates better with its conduction performance: 13 mS/cm at 150ºC for pristine PBI cast from 190 kDa commercial Fumion APH vs. 18 mS/cm at 150ºC for PBI membrane cast from 105.1 kDa polymer and 4.7 as doping level [35].

Con formato: Sin subrayado

Con formato: Sin subrayado

Con formato: Sin subrayado

Con formato: Sin subrayado

Con formato: Sin subrayado

Con formato: Sin subrayado

Con formato: Sin subrayado

Con formato: Sin subrayado

Con formato: Sin subrayado

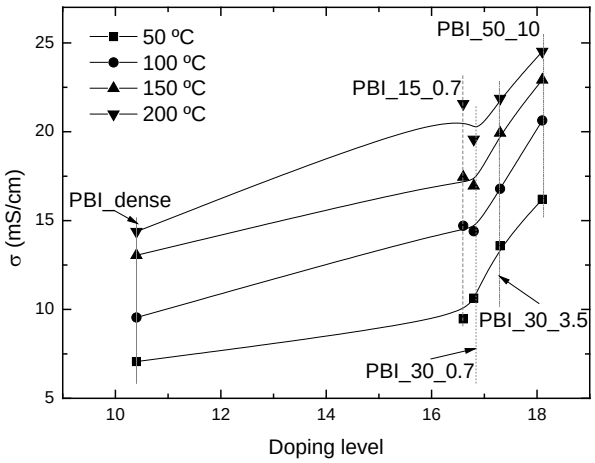

Figure 9. Proton Conduction performance of TE PBI membranes as a function of H_3PO_4 doping level.

Nevertheless, the exhibited pattern by TE samples with porosity above 0.7% clearly differs from pristine and low irradiated samples. More specifically, the conductivity-doping level dependence is more noticeable for highly irradiated membranes. Once again, this experimental observation is

underlying the physico-chemical modification of PBI films by heavy irradiation with positive impact on conduction performance. Thus, the radiochemical PBI cross-linking in the surroundings of tracks provides with additional H-bonding interactions among neighbouring chains due to closer inter-chain distances (i.e. low free volume domains). Furthermore, the PBI chain scission provides with randomly arranged benzimidazole fragments (i.e. high free volume domains) enriched in–NH groups as donor-acceptor proton sites.

Therefore, these two extra contributions have to be considered in addition to the presence of free phosphoric acid molecules on the pore walls for a proper understanding of the proton transport through TE membranes. Our postulated conduction mechanism for TE membranes, illustrated in Figure 10, involves a new dynamic hydrogen bonding network of shorter benzimidazole fragments, cross-linked nanodomains and free amphoteric phosphoric acid molecules settled on the pore walls.

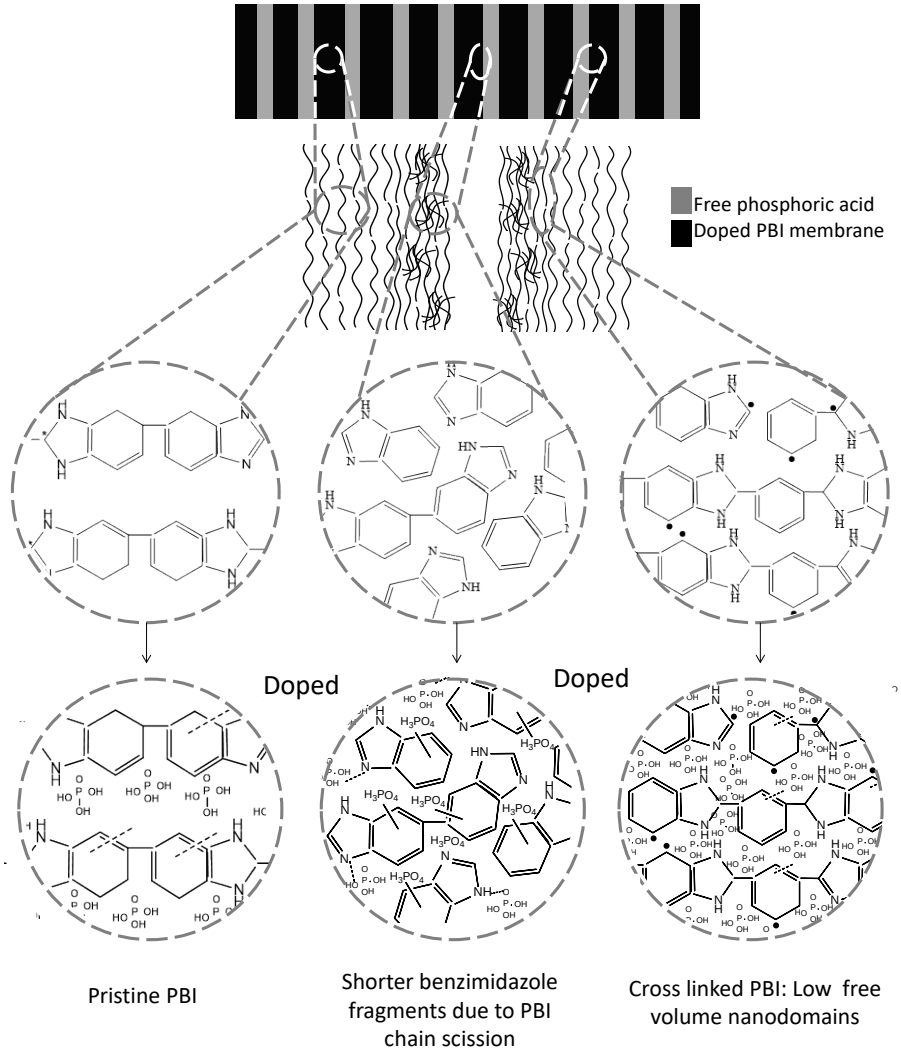

Figure 10. Postulated conduction mechanism for phosphoric acid doped TE PBI membranes.

Con formato: Sin subrayado

The existence of this additional donor-acceptor hydrogen network is responsible not only for the conductivity promotion but also for the lower activation energy values exhibited by irradiated samples. Figure 11 shows the Arrhenius plot of conductivity in the high temperature operating window (above 120^{o}C). The as calculated activation energy (Ea) values for the proton conduction mechanism were in the following order: 8.2 kJ/mol for PBI> 4.8 kJ/mol for PBI_30_0.7 >4.3 kJ/mol for PBI_15_0.7> 3.5 kJ/mol for PBI_30_3.5 > 2.1 kJ/mol for PBI_50_10.

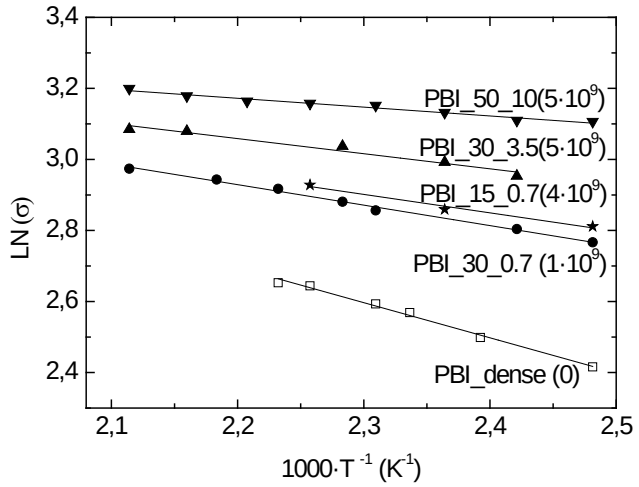

Figure 11. Arrhenius Conductivity plot for the phosphoric acid doped TE PBI membranes.

In Figure 12 the Arrhenius type activation energy is plotted against the external surface area calculated from the pore density (pores per cm^2 of top membrane surface) and the external area of each pore (pore diameter·π·membrane thickness). A clear linear relationship for TE samples is attained supporting the benefits of ion beaming on conductivity properties. Nevertheless, the beaming conditions are somewhat constrained by the mechanical properties of the resulting membranes. Accordingly, the most outstanding TE membrane prepared in this work is PBI_50_10.

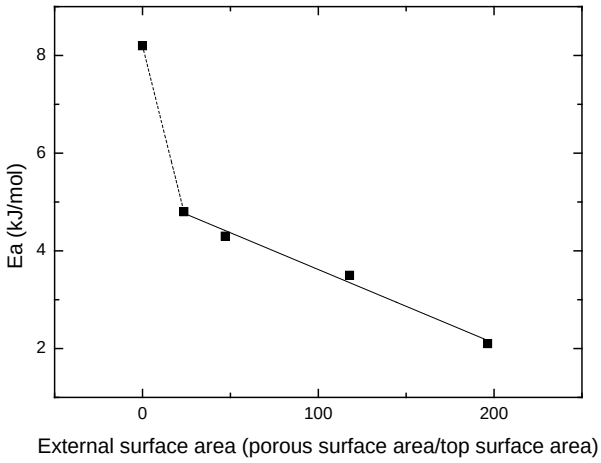

Figure 12. Relationship between Arrhenius type Activation Energy for proton transport and external surface area of TE PBI membranes.

For the assessment of endurance properties, extended through-plane conductivity experiments (up to 240 h) have been carried out at 150^{o}C in presence of 0.05 water molar fraction (see Figure 13). A first decay in performance (about 9 %) takes place after 24 h operation time. These conductivity losses are associated with autodehydration process of phosphoric acid, as evidenced the differential thermograms shown in Figure 9. Afterwards, the conductivity progressively decreases (about 23 %), reaching almost a steady-state plateau after 150 h operation time. According to TGA results performed on TE samples after conductivity tests (not shown here), the second decay is attributed to the dragging of free acid molecules from the nanopores. These proton conductivity values, varying from 15 mS/cm for PBI_30_0.7 to 18 mS/cm for PBI_50_10, are almost three folds higher than the exhibited by pristine PBI.

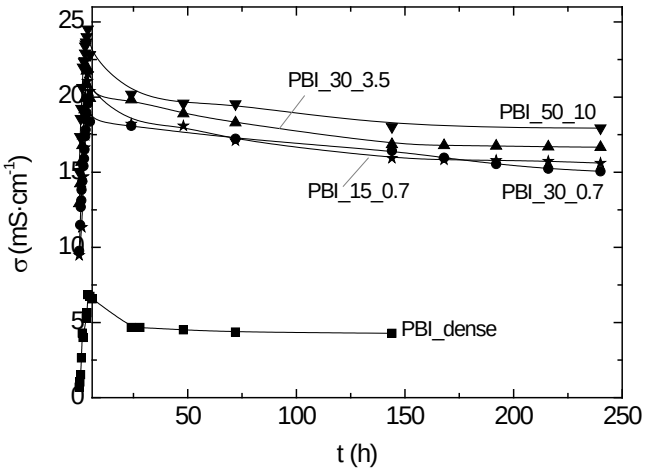

Figure 13. Durability test for the phosphoric acid doped TE PBI membranes at 150^{o}C in presence of 0.05 water molar fraction.

4. Conclusions

Novel electrolyte membranes based on phosphoric acid doped track-etched polybenzimidazole (PBI) films have been deployed for the first time as proton electrolyte membranes for high temperature applications. TE PBI membranes with end pore diameters varying from 15 to 50 nm have been successfully obtained. The maximum overall membrane porosity is 10% due to the random in plane track distribution determines the mechanical properties of the resulting films. On the other hand, porosity values lower than 0.7% are recommended to alleviate the pore coalescence phenomena. On the basis of physico chemical characterization results for irradiated samples, Xe beaming is modifying the polymeric network by chain scission phenomena leading to shorter polymer chains with better mobility. Besides, the plastic deformation induced by ion beaming also anticipates the PBI decomposition/degradation. Such chemical modification of PBI skeleton is also responsible for the enhanced phosphoric acid embedding process. Accordingly, PBI_50_10 membrane, 50 nm as end pore diameter and $5 \cdot 10^{9}$ cm^{-2} as pore density, seems the most adequate for high temperature PEM applications exhibiting conductivities values above 15 mS/cm at 150^{o}C after 250 h operation time. These encouraging results also pave the way for potential applications in gas-vapor separation and liquid filtration under harsh pH and temperature conditions.

Con formato: Sin subrayado

Con formato: Sin subrayado

Con formato: Sin subrayado

Con formato: Sin subrayado

Con formato: Sin subrayado

Acknowledgements

The authors would like to acknowledge financial support from the European Commission through the FP7 funded project ZEOCELL (http://ina.unizar.es/zeocell): Grant Agreement no: 209481.

Con formato: Sin subrayado

References

[1] http://eur-lex.europa.eu/LexUriServ/LexUriServ.do?uri=COM:2010:0639:FIN:EN:HTML. Communication from the commission to the European Parliament, the council, the european economic and social Committee and the committee of the regions. Energy 2020: A strategy for competitive, sustainable and secure energy. Accessed on July 2013.

[2] S. Bose, T. Kuila, T.X.H. Nguyen, N.H. Kim, K.-t. Lau, J.H. Lee, Polymer membranes for high temperature proton exchange membrane fuel cell: Recent advances and challenges, Progress in Polymer Science, 36 (2011) 813-843.

[3] J.A. Asensio, E.M. Sanchez, P. Gomez-Romero, Proton-conducting membranes based on benzimidazole polymers for high-temperature PEM fuel cells. A chemical quest, Chemical Society Reviews, 39 (2010) 3210-3239.

[4] Q. Li, J.O. Jensen, R.F. Savinell, N.J. Bjerrum, High temperature proton exchange membranes based on polybenzimidazoles for fuel cells, Progress in Polymer Science, 34 (2009) 449-477.

[5] H. Steininger, M. Schuster, K.D. Kreuer, A. Kaltbeitzel, B. Bingol, W.H. Meyer, S. Schauff, G. Brunklaus, J. Maier, H.W. Spiess, Intermediate temperature proton conductors for PEM fuel cells based on phosphonic acid as protogenic group: A progress report, Physical Chemistry Chemical Physics, 9 (2007) 1764-1773.

[6] M.K. Daletou, N. Gourdoupi, J.K. Kallitsis, Proton conducting membranes based on blends of PBI with aromatic polyethers containing pyridine units, Journal of Membrane Science, 252 (2005) 115-122.

[7] T. Omata, M. Tanaka, K. Miyatake, M. Uchida, H. Uchida, M. Watanabe, Preparation and Fuel Cell Performance of Catalyst Layers Using Sulfonated Polyimide Ionomers, ACS Applied Materials & Interfaces, 4 (2011) 730-737.

[8] S. Angioni, P.P. Righetti, E. Quartarone, E. Dilena, P. Mustarelli, A. Magistris, Novel aryloxy-polybenzimidazoles as proton conducting membranes for high temperature PEMFCs, International Journal of Hydrogen Energy, 36 (2011) 7174-7182.

[9] S.-W. Chuang, S.L.-C. Hsu, M.-L. Yang, Preparation and characterization of fluorine-containing polybenzimidazole/imidazole hybrid membranes for proton exchange membrane fuel cells, European Polymer Journal, 44 (2008) 2202-2206.

[10] Y. Guan, H. Pu, D. Wan, Synthesis and properties of poly[2,2[prime or minute]-(4,4[prime or minute]-(2,6-bis(phenoxy) benzonitrile))-5,5[prime or minute]-bibenzimidazole] for proton conducting membranes in fuel cells, Polymer Chemistry, 2 (2011) 1287-1292.

[11] S.J. Park, D.H. Lee, Y.S. Kang, High temperature proton exchange membranes based on triazoles attached onto SBA-15 type mesoporous silica, Journal of Membrane Science, 357 (2010) 1-5.

[12] S.-K. Kim, T.-H. Kim, J.-W. Jung, J.-C. Lee, Polybenzimidazole containing benzimidazole side groups for high-temperature fuel cell applications, Polymer, 50 (2009) 3495-3502.

[13] N. Tan, G. Xiao, D. Yan, G. Sun, Preparation and properties of polybenzimidazoles with sulfophenylsulfonyl pendant groups for proton exchange membranes, Journal of Membrane Science, 353 (2010) 51-59.

[14] Z. Xia, S. Yuan, G. Jiang, X. Guo, J. Fang, L. Liu, J. Qiao, J. Yin, Polybenzimidazoles with pendant quaternary ammonium groups as potential anion exchange membranes for fuel cells, Journal of Membrane Science, 390–391 (2012) 152-159.

[15] S.C. Kumbharkar, P.B. Karadkar, U.K. Kharul, Enhancement of gas permeation properties of polybenzimidazoles by systematic structure architecture, Journal of Membrane Science, 286 (2006) 161-169.

[16] S.-K. Kim, T.-H. Kim, T. Ko, J.-C. Lee, Cross-linked poly(2,5-benzimidazole) consisting of wholly aromatic groups for high-temperature PEM fuel cell applications, Journal of Membrane Science, 373 (2011) 80-88.
[17] R.L. Fleischer, P.B. Price, E.M. Symes, Novel Filter for Biological Materials, Science, 143 (1964) 249-250.
[18] R.R.L. Fleischer, P.B. Price, R.M. Walker, Nuclear tracks in solids: principles and applications, Univ of California Press, 1975.
[19] P. Apel, Track etching technique in membrane technology, Radiation Measurements, 34 (2001) 559-566.
[20] S.K. Chakarvarti, Track-etch membranes enabled nano-/microtechnology: A review, Radiation Measurements, 44 (2009) 1085-1092.
[21] E. Ferain, R. Legras, Pore shape control in nanoporous particle track etched membrane, Nuclear Instruments and Methods in Physics Research Section B: Beam Interactions with Materials and Atoms, 174 (2001) 116-122.
[22] E. Ferain, R. Legras, Track-etch templates designed for micro- and nanofabrication, Nuclear Instruments and Methods in Physics Research Section B: Beam Interactions with Materials and Atoms, 208 (2003) 115-122.
[23] C. Trautmann, W. Brüchle, R. Spohr, J. Vetter, N. Angert, Pore geometry of etched ion tracks in polyimide, Nuclear Instruments and Methods in Physics Research Section B: Beam Interactions with Materials and Atoms, 111 (1996) 70-74.
[24] C. Trautmann, S. Bouffard, R. Spohr, Etching threshold for ion tracks in polyimide, Nuclear Instruments and Methods in Physics Research Section B: Beam Interactions with Materials and Atoms, 116 (1996) 429-433.
[25] L. Klintberg, M. Lindeberg, G. Thornell, Sodium hypochlorite as a developer for heavy ion tracks in polyimide, Nuclear Instruments and Methods in Physics Research Section B: Beam Interactions with Materials and Atoms, 184 (2001) 536-543.
[26] A.I. Vilensky, V.V. Berezkin, V.D. Sobolev, K.G. Sabbatovsky, Y.K. Kochnev, S.V. Vlasov, V.R. Flid, A.B. Vasilyev, A.Y. Kolesnikov, V.V. Medvedev, B.V. McHedlishvili, Pore formation in polyimide irradiated by high-energy ions and the properties of the obtained membranes, Colloid J, 71 (2009) 466-469.
[27] R. Koivula, S. Makkonen-Craig, R. Harjula, M. Paronen, Ion exchange properties of sulfonated polycarbonate and polyimide track etch membranes, Reactive and Functional Polymers, 72 (2012) 92-97.
[28] M. Ali, B. Schiedt, K. Healy, R. Neumann, W. Ensinger, Modifying the surface charge of single track-etched conical nanopores in polyimide, Nanotechnology, 19 (2008) 085713.

[29] A. Eguizábal, J.Lemus, M. Urbiztondo, O. Garrido, J. Soler, A.Blazquéz, M.P. Pina, Novel Hybrid Membranes based on Polybenzimidazole and ETS-10 titanosilicate type material for High Temperature PEMFCs: a comprehensive study on dense and porous systems, Journal of Power Sources, 196 (2011) 8994–9007.

[30] A. Eguizábal, J.Lemus, V. Roda, M. Urbiztondo, F. Barreras, M.P. Pina, Nanostructured electrolyte membranes based on zeotypes, protic ionic liquids and porous PBI membranes: Preparation, characterization and MEA testing, International Journal of Hydrogen Energy, 37 (2012) 7221–7234.

[31] A. Kros, R.J. Nolte, N. Sommerdijk, Conducting polymers with confined dimensions: Track-etch membranes for amperometric biosensor applications, Advanced Materials, 14 (2002) 1779-1782.

[32] T. Sancho, J. Soler, M.P. Pina, Conductivity in zeolite-polymer composite membranes for PEMFCs, Journal of Power Sources, 169 (2007) 92-97.

[33] S. Ghosh, R. Klett, D. Fink, K.K. Dwivedi, J. Vacik, V. Hnatowicz, J. Cervena, On the penetration of aqueous solutions into pristine and radiation damaged polyimide, Radiation Physics and Chemistry, 55 (1999) 271-284.

[34] D. Fink, R. Klett, L.T. Chadderton, J. Cardoso, R. Montiel, H. Vazquez, A.A. Karanovich, Carbonaceous clusters in irradiated polymers as revealed by small angle X-ray scattering and ESR, Nuclear Instruments and Methods in Physics Research Section B: Beam Interactions with Materials and Atoms, 111 (1996) 303-314.

[35] J. Lobato, P. Cañizares, M.A. Rodrigo, J.J. Linares, J.A. Aguilar, Improved polybenzimidazole films for H_3PO_4-doped PBI-based high temperature PEMFC, Journal of Membrane Science, 306 (2007) 47-55.

Con formato: Sin subrayado

Con formato: Sin subrayado

Con formato: Sin subrayado

Con formato: Sin subrayado

Con formato: Sin subrayado

Table List

Con formato: Sin subrayado

Figure Captions

Figure 1. Track-etching process for the production of porous membranes from polymer films.

Figure 2. PBI films 50 μm thick after chemical etching: left) 2M KOH solution at 80ºC; right) 2M NaOCl solution at 65ºC.

Figure 3. Top view of nanoporous TE PBI membranes: A) PBI_30_0.7; B) PBI_30_3.5; B) PBI_50_10.

Figure 4 TEM analyses of pore size variation with the depth in the PBI_30_0.7 sample: A) top surface, B) 10 μm to the top surface; and the PBI_15_0.7 sample: C) top surface, D) 10 μm to the top surface.

Figure 5.A. FTIR analysis in the 1550-1150 cm^{-1} region for TE PBI membranes with different pore density values: a) pristine PBI; b) PBI_30_0.7 ($1 \cdot 10^9$ cm^{-2}); c) PBI_30_3.5 ($5 \cdot 10^9$ cm^{-2}); d) PBI_50_10 ($5 \cdot 10^9$ cm^{-2}).

Figure 5.B. FTIR analysis in the 1050-750 cm^{-1} region for TE PBI membranes with different pore density values: a) pristine PBI; b) PBI_30_0.7 ($1 \cdot 10^9$ cm^{-2}); c) PBI_30_3.5 ($5 \cdot 10^9$ cm^{-2}); d) PBI_50_10 ($5 \cdot 10^9$ cm^{-2}).

Figure 5.C. FTIR analysis in the 3700-2900 cm^{-1} region for TE PBI membranes with different pore density values: a) pristine PBI; b) PBI_30_0.7 ($1 \cdot 10^9$ cm^{-2}); c) PBI_30_3.5 ($5 \cdot 10^9$ cm^{-2}); d) PBI_50_10 ($5 \cdot 10^9$ cm^{-2}).

Figure 6. DSC analyses for some of the TE PBI membranes prepared in this work: A) Influence of track etching on Tg values; B) Removal of carbonaceous by-products generated during beaming with chemical etching step.

Con formato: Sin subrayado

Figure 7. Top view of phosphoric acid doped PBI_30_0.7 membrane as a function of doping time: A) 0 h; B) 0,5 h; C) 6h; D) 24 h (pore coalescence is observed).

Figure 8. Differential TGA for phosphoric acid doped PBI_50_10 and pristine PBI samples.

Figure 9. Proton Conduction performance of TE PBI membranes as a function of H_3PO_4 doping level.

Figure 10. Postulated conduction mechanism for phosphoric acid doped TE PBI membranes.

Figure 11. Arrhenius Conductivity plot for the phosphoric acid doped TE PBI membranes.

Figure 12. Relationship between Arrhenius type Activation Energy for proton transport and external surface area of TE PBI membranes.

Figure 13. Durability test for the phosphoric acid doped TE PBI membranes at 150ºC in presence of 0.05 water molar fraction.